Northumbria
University
NEWCASTLE

New Journal of Chemistry

ARTICLE

Black phosphorus nanosheet-polypyrrole nanocomposites for high-performance photothermal cancer therapy

Chengkang Su,[#a] Huiqing Zhong,[#a] Haolin Chen,[b] Yanxian Guo,[a] Zhouyi Guo,[a] Deqiu Huang,[a] Wen Zhang,[a] Qiang Wu,[*c] Biwen Yang[d] and Zhiming Liu[*a]

The favorable biocompatibility, biodegradability and broadband absorption from ultraviolet to near-infrared (NIR) region have endowed black phosphorus (BP), the new generation of two-dimensional nanomaterials, with great potential for photothermal therapy (PTT). However, an appropriate but not low dosage of nanoagent is requisite to achieve the satisfactory therapeutic effect in BP-based NIR PTT, due to the decreasing light absorption of BP in NIR region. In this work, the nanohybrids consist of BP nanosheets and several polypyrrole (PPy) nanoparticles attached to them (BP/PPy NSs) are fabricated for high-performance NIR PTT, benefiting from the superimposed NIR absorption characteristics of the two components. The nanocomposites exhibit irregular, speckled and flake-like morphologies with good biocompatibility and superior NIR photothermal transduction efficiency compared with that of bare nanosheet. The utlization of BP/PPy NSs as novel nanotherapeutic agents for enhanced NIR photothermal cancer therapy are accomplished *in vitro* and *in vivo*.

1. Introduction

The treatment of cancer has become research focus in the world today due to its high morbidity and mortality.[1-3] As a promising supplement to surgery, radiotherapy, chemotherapy, and other major clinical therapies, photothermal therapy (PTT) that delivers phototherapeutic agents into tumor cells to convert photons into heat to achieve the ablation of tumor is a minimally invasive treatment for tumors.[4-6] Recently, many systems, such as noble metal nanoparticles, carbon nanomaterials, conducting polymers, and organic dye molecules, have been explored as PTT agents for cancer treatment.[7-14] However, their applications are often limited by low photothermal conversion efficiency, high cost, high systemic cytotoxicity, or undesirable photostability.

As an emerging inorganic two-dimensional (2D) nanomaterial, black phosphorus (BP) with a peculiar structure and a layer-dependence bandgap of 0.3-2.0 eV, has aroused enormous concern in the fields of electro-/photocatalysis, energy storage, photodetectors and chemo-/biosensing.[15-17] More recently, BP nanosheets (NSs) have been exploited as a promising nanotheranostic agent for several biomedical applications, which benefited from its good biodegradability and ingenious physicochemical properties.[18-21] As a typical 2D nanomaterial, BP possesses broadband light absorption from ultraviolet to near-infrared (NIR) region that has been developed as the "heat messenger" for NIR photothermal tumor therapy.[22-25] BP NSs can also serve as the nanoplatform to carry drugs, organic molecules or nanoparticles for fabrication of multifunctional nanosystems which allows the multimodal theranostic applications integrating PTT and chemotherapy, photodynamic therapy, bioimaging or biosensing.[26-31] An unavoidable fact that the declining optical absorption in NIR region requires BP to reach a certain dose in PTT treatment, which, however, arouses the concern over the biosafety of nanomaterials.[32] It has been proven that bare BP NSs could be captured by macrophages, resulting in significant inflammatory responses.[33] BP can also adsorb immune relevant proteins *in vitro*, further trigger immunotoxicity and immune perturbation in macrophages.[34] The cytotoxicity induced by BP NSs shows concentration- and size- dependency, probably be considered as the result of the generation of intracellular reactive oxygen species and plasma membrane damage induced by BP nanomaterials.[35] Therefore, reasonable strategies for fabrication of BP-based nanoplatforms with minor BP usage while not affecting their NIR features is highly encouraged.

Polypyrrole (PPy), a type of highly biocompatible conducting polymer, exhibits strong and broad absorption in the NIR region, and has been applied as the PTT nanoagent for cancer therapy.[36-38] Monodispersed PPy nanoparticles (NPs) can be readily prepared by one-pot oxidative polymerization approaches in the presence of water-soluble polymers.[39, 40] It has been reported that PPy showed higher photothermal

[a] *MOE Key Laboratory of Laser Life Science & SATCM Third Grade Laboratory of Chinese Medicine and Photonics Technology, College of Biophotonics, South China Normal University, Guangzhou 510631, Guangdong, China. E-mail: liuzm021@126.com*

[b] *Key Laboratory of Sensing Technology and Biomedical Instrument of Guangdong Province, School of Biomedical Engineering, Sun Yat-sen University, Guangzhou, Guangdong 510006, P. R. China.*

[c] *Faculty of Engineering and Environment, Northumbria University, Newcastle NE1 8ST, UK. E-mail: qiang.wu@northumbria.ac.uk*

[d] *Guangzhou Micro-shot Technology Co., Ltd, Guangzhou 510640, Guangdong, China.*

#These authors contributed equally to this work.

Electronic Supplementary Information (ESI) available: [details of any supplementary information available should be included here]. See DOI: 10.1039/x0xx00000x

conversion efficiency and better photostability under NIR irradiation compared with those of most reported materials.[37, 40] Furthermore, *in vitro* and *in vivo* studies have confirmed the good biocompatibility of PPy after a long-term monitoring.[41, 42] Herein, nanocomposites integrated BP NSs with spherical PPy NPs (BP/PPy NSs) are fabricated through a facile one-step approach. A biocompatible stabilizer, polyethylene glycol (PEG), is also utilized to improve the dispersity in liquid environment. The deposition of PPy NPs onto BP sheets remarkably promote the absorption of nanostructures in NIR region, which enables the enhanced NIR photothermal tumor therapy *in vitro* and *in vivo*. Our results inspire the ingenious strategies for the further explorations of BP-based nanomedicine.

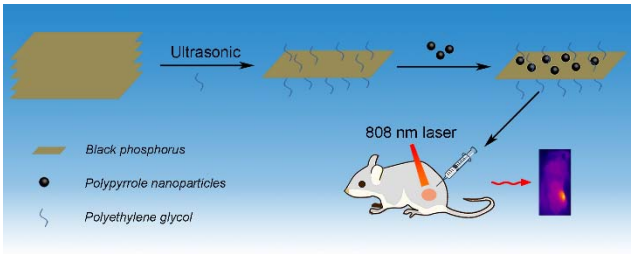

Scheme 1 Schematic illustration of preparation of BP/PPy NSs and their enhanced photothermal tumor therapeutic application.

2. Materials and methods

2.1 Materials

The bulk BP crystals were purchased from XFNANO Materials Tech Co. Ltd (Nanjing, China) and stored in a dark Ar-filled glovebox. $FeCl_3$, pyrrole monomer, N-methyl-2-pyrrolidone (NMP) and polyvinylpyrrolidone (PVP) were obtained from China National Medicine Corporation (Shanghai, China). Roswell Park Memorial Institute (RPMI)-1640, trypsin, methylthiazolyldiphenyl-tetrazolium bromide (MTT), and fetal bovine serum (FBS) were obtained from GIBCO (Grand Island, NY, United States). Methoxy-polyethylene glycol-amine (mPEG-NH_2, Mw 5000) was purchased from Shanghai Aladdin Reagent Co., Ltd. Other reagents were purchased from China National Medicine Corporation and used as received. Deionized water was used in all experiments. (Milli-Q System, Millipore, USA).

2.2 Synthesis of BP/PPy NSs

The BP NSs were obtained by the liquid exfoliation method [22]. In brief, 30 mg of the bulk BP powders were dispersed in 30 mL of NMP under ice water bath ultrasonication with a sonic tip (600 W) for 6 h (2 s duration and 4 s interval). Then the mixture was sonicated 10 h in an ice bath using a power of 300 W. The dispersion was centrifuged for 20 min at 7000 rpm to get the precipitation. The final product was then obtained by centrifugation (2000 rpm, 20 min), and the supernatant was resuspended in NMP for further use. PEGylated BP NSs were prepared through electrostatic bonding. 10 mg mPEG-NH_2 were dispersed in the 10 mL of BP solution (200 μg/mL), then the mixture was sonicated for 30 min, and then stirred for 4 h. The as-prepared BP NSs were collected by centrifugation at 7000 rpm for 20 min to remove the unreacted PEG-NH_2. Finally, BP NSs were dispersed in the ultrapure water at 4 °C.

Polypyrrole nanoparticles with narrow size distribution were readily prepared via chemical oxidation polymerization.[40] Briefly, 1 g of PVP was dissolved in 25 mL ultrapure water in a 50 mL sealed container by stirring at room temperature for 0.5 h. 130 μL of monomer pyrrole was added to the solution. After 10 min, 1 mL of 0.75 g/mL $FeCl_3$ was quickly added to the reaction mixture. The polymerization was performed for another 3 h. Then, the products were purified by washing with ethanol-acetone mixture and finally redispersed in ultrapure water. To prepare BP/PPy NSs, 100, 200 or 300 μL of above prepared PPy solution was added into 10 mL of BP NSs solution and stirred in the dark for 6 h. Then the mixture solution was centrifuged at a speed of 7000 rpm for 20 min, then resuspended in ultrapure water.

2.3 Characterization

The morphologies of the nanostructures were observed by the atomic force microscope (AFM, FM-Nanoview 1000, FSM-Precision, China) and the transmission electron microscope (TEM, JEM-2100HR, JEOL, Japan). The UV-vis-NIR absorption spectra were recorded on a spectrophotometer (UV-6100, MAPADA, China). Raman spectra were obtained using a Renishaw inVia microspectrometer (Derbyshire, England) equipped with the excitation wavelength of 514.5 nm generated by an Ar+ laser.

2.4 Photothermal heating experiments

BP NSs and BP/PPy NSs suspensions were irradiated with a continuous-wave diode NIR laser (808 nm, Changchun New Industries Optoelectronics Technology, China) with a power density of 2 W/cm². The temperatures of the solutions were measured every 30 s using the infrared thermal camera (Fluke Ti200, Fluke Corp, Washington, USA). To evaluate the photothermal stability, the nanostructure solutions were exposed to NIR laser for 5 min (laser on), followed by naturally decreased to room temperature after the laser was turned off (laser off); this procedure was repeated five times.

2.5 *In vitro* experiments

4T1 murine breast cancer cells were cultured in RPMI-1640 cell medium supplemented with 10 % fetal bovine serum (FBS), penicillin (100 units/mL), and streptomycin (100 μg/mL) in 5% CO2 and 95% air at 37 °C in a humidified incubator. For cytotoxicity analysis, 4T1 cells were plated into 96-well plates for 12 h incubation. Then the medium was replaced with 100 μL of fresh RPMI-1640 containing BP NSs or BP/PPy NSs with different concentrations for another 24 h incubation. The cell viabilities were finally measured by the classic MTT assay.

In order to assess the *in vitro* photothermal effects of BP NSs and BP/PPy NSs, 4T1 cells were randomly divided into four groups (Control, Laser, BP NSs + Laser, BP/PPy NSs + Laser). After cells adhered onto the cell plate, the medium was replaced with fresh RPMI-1640 containing different concentrations of BP NSs or BP/PPy NSs (5, 10, 20 and 30 μg/mL), respectively. After 6 h of incubation, the cells were irradiated

with an 808 nm continuous-wave NIR laser with the power density of 2 W/cm^2 for 2 min and then incubated in a humidified incubator for 24 h. Finally, the cell viabilities were measured by the MTT assay. The antitumor effects of BP nanomaterials were also measured by the fluorescence imaging analysis. The cells 4 h after NIR laser exposure were fixed with 4% formalin buffered in the PBS for 10 min. After washing three times with PBS, the 4T1 cells were stained with Hoechst 33258 dye (4 μg/mL) for 10 min. The apoptotic cells were observed using a fluorescence microscopy.

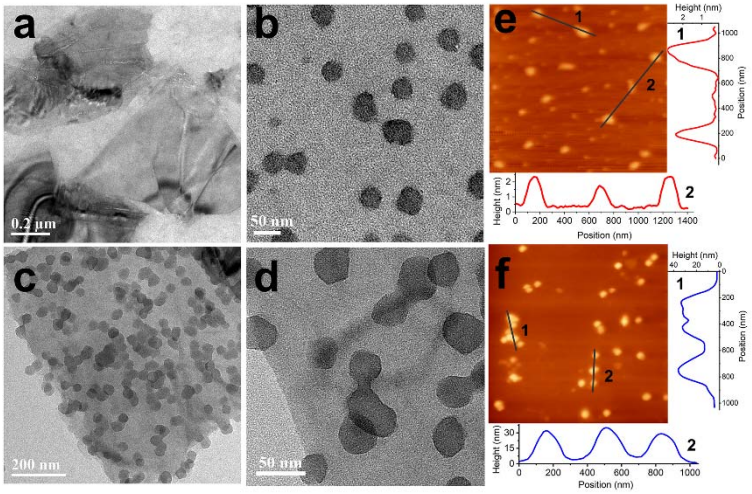

Fig. 1 TEM images of a) BP NSs, b) PPy NPs and c, d) BP/PPy NSs, respectively. AFM images of e) BP NSs and f) BP/PPy NSs with the corresponding height profiles along the lines.

2.6 In vivo antitumor effect

24 female Balb/c mice (6 weeks old) were obtained from the Laboratory Animal Centre, Sun Yat-sen University. All experiments were conducted under protocols approved by the South China Normal University Animal Care and Use Committee. 100 μL 4T1 cells (2 × 10^6) were injected into the flank region of the Balb/c mice. Animal experiments started when the tumor volume reached about 200 mm^3. For *in vivo* photothermal therapy, tumor-bearing mice were randomly divided into four groups (Control, PBS + Laser, BP NSs + Laser, BP/PPy NSs + Laser), minimizing the differences of weight and tumor sizes in each group. After intratumoral injection of 100 μL nanomaterials (1 mg/kg) for 12 h, the tumor regions of the mice were irradiated with 808 nm laser (2 W/cm^2) for 2 min. During the laser irradiation, the surface temperature of the tumor was monitored by an infrared thermal camera. The tumor sizes were measured by a digital caliper every the other day and calculated as the volume = (tumor length) × (tumor width)^2/2. Relative tumor volume was calculated as V/V_0 (V_0 was the tumor volume at the beginning of the experiment). In order to assess the *in vivo* toxicities of nanomaterials, the mice were sacrificed after 17 days' treatment, then the major organs (spleen, liver, kidney, heart and lung) of mice from each group were collected, and fixed into 4% neutral formaldehyde, conducted with paraffin embedded sections, stained by hematoxylin and eosin (H&E), and observed under a microscope.

3. Results and Discussion

3.1 Synthesis and Characterization of BP/PPy NSs

Scheme 1 shows the schematic illustration of the synthesis of BP/PPy NSs and their antitumor effect. Classic ultrasonic stripping method was adopted to prepare the BP nanosheets. As described in Fig. 1a, the TEM image of BP NSs shows flake-like morphology with single or few layers. The lamellar structure of BP NSs can also be confirmed by the AFM analysis, indicating an average height of around 2.1 nm (Fig. 1e). Spherical PPy NPs were synthesized by oxidation polymerization using PVP as the capping agent, which exhibited1 a mean size about 40 nm (Fig. 1b). Fig. 1c and d display the morphological features of BP/PPy NSs, where the surface of BP sheets is attached with a large number of PPy NPs with random distribution. Almost all nanoparticles are confined in the nanoplatform showing the successfully attachment of PPy NPs onto the BP nanosheets. The deposition of PPy NPs significantly increases mean height of BP/PPy NSs (Fig. 1f). The lateral lengths of the BP nanostructures are calculated to be about 330 nm (Fig. S1† and S2†).

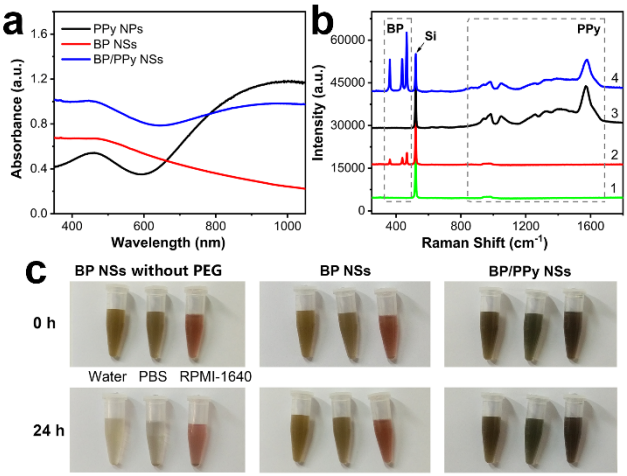

Fig. 2 a) UV-vis-NIR absorbance spectra of the nanomaterials. b) Raman spectra of Si substrate (1), BP NSs (2), PPy NPs (3) and

BP/PPy NSs (4). c) The stability of the nanostructures in water, PBS and RPMI-1640, respectively.

The UV-vis-NIR spectrum of BP NSs (Fig. 2a) displays an obviously decreasing light absorption from UV to NIR region, which agrees with those of other 2D layered nanomaterials.[9] In marked contrast, an increasing optical absorption in NIR region is observed in the UV-vis-NIR spectrum of PPy NPs with a broad peak at ~910 nm. The deposition of PPy NPs onto the 2D nanosheets endows the nanohybrids with a significantly increased optical absorption in the NIR region, indicating the promising potential for photothermal cancer therapy. Raman spectrum were performed to research on the chemical structures of nanomaterials. As shown in the Fig. 2b, three typical Raman peaks at about 361 cm^{-1}, 438 cm^{-1} and 466 cm^{-1} are observed in the Raman spectrum of BP NSs, which can be assigned to A_g^1, B_{2g}, and A_g^2 modes of BP NSs, respectively.[22] Compared with BP NSs, the Raman spectrum of BP/PPy NSs shows another peaks located at 986 cm^{-1}, 1040 cm^{-1}, 1315 cm^{-1} and 1566 cm^{-1}, which can be ascribed to the combination of PPy NPs (Fig. 2b).[43] The stability test shows a poor dispersity and stability of BP NSs in water, PBS and RPMI-1640, respectively (Fig. 2c, Fig. S3†). After PEGylation, the nanomaterials (BP NSs and BP/PPy NSs) become more stable with a tiny amount of nanostructures are precipitated during the 24 h of observation.

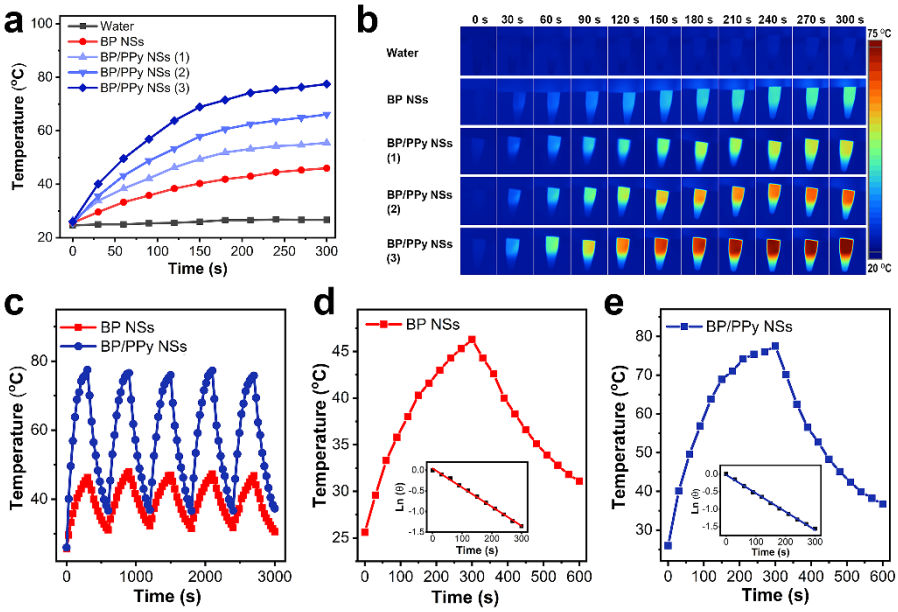

Fig. 3 a) Temperature curves and b) corresponding infrared thermal images of BP/PPy NSs solutions (20 μg/mL) with different weight ratios of BP and PPy exposed to 808 nm laser at a power density of 2 W/cm^2. c) Temperature variations of BP NSs and BP/PPy NS solutions under five times of laser on/off cycles. Plots of the temperature vs time for d) BP NSs and e) BP/PPy NS during laser irradiation and cooling (laser off). Insets show the fitting curves of cooling time vs ln(θ).

3.2 Photothermal Properties of BP/PPy NSs

BP NSs and BP/PPy NSs at the same concentrations were exposed to an 808 nm NIR laser with a power density of 2.0 W/cm^2 to evaluate the photothermal properties of the nanomaterials. The temperatures were monitored by an infrared thermal camera as a function of irradiation. As shown in Fig. 3a, the BP NSs and BP/PPy NSs solutions both experience fast increases of temperature during the NIR irradiation. While the nanohybrids generate heat more efficiently (ΔT ≈ 52 °C, 5 min) than BP NSs (ΔT ≈ 20 °C), illustrating a better NIR photothermal transduction efficiency. We also observe that the amount of PPy nanoparticles on the surface of BP nanosheet plays a critical role in the increase of heat generation. The corresponding infrared thermal images of the solutions also show the changes in temperature during laser exposure (Fig. 3b). BP/PPy NSs (3) was chose for the further investigation because of its best photothermal feature. To evaluate the photothermal stability of the BP/PPy NSs, we monitored the temperature of BP/PPy NSs under NIR laser for 5 min (laser on), followed by natural cooling to room temperature, and the heating-cooling process were repeated five times. As shown in Fig. 3c, that the highest temperature of BP/PPy NSs under NIR exposure remains unchanged during the five cycles, indicating an excellent photothermal stability. For exact explanation of the photothermal properties of BP NSs and BP/PPy NSs, the photothermal conversion efficiencies (η) were calculated using the following Eqs.[44, 45]

$$\eta = \frac{hS(T_{max} - T_{surr}) - Q_{dis}}{I(1-10^{-A_{808}})} \quad (1)$$

$$hS = \frac{m_D C_D}{\tau_s} \quad (2)$$

$$\tau_s = \frac{-t}{\ln\theta} \quad (3)$$

$$\theta = \frac{T_{surr} - T}{T_{surr} - T_{max}} \quad (4)$$

where h was the heat transfer coefficient, S was the surface area of the container, I expressed the NIR laser power (808 nm, 2.0 W/cm^2), A_{808} meant the absorbance at 808 nm of the nanostructures (OD_{BP}=0.36, $OD_{BP/PPy}$=0.91), the equilibrium temperature was T_{max}, the ambient temperature of the surroundings was T_{surr}, and the heat associated with the light absorbance by the solvent was Q_{dis}. τ_s represented the sample

system time constant, m_D and C_D meant the mass (1.0 g) and heat capacity (4.2 J/g), when pure water was used as the solvent. Pure water in a test tube was applied to measure the Q_{dis}. As displayed in Fig. 3d and e, the time constants are determined to be 216 s and 191 s for BP NSs and BP/PPy NSs solutions, respectively. Then, the η value of BP/PPy NSs is calculated to be 62.2%, significantly higher than that of BP NSs (31.8%), which further confirms the remarkably enhanced NIR photothermal property of BP/PPy NSs.

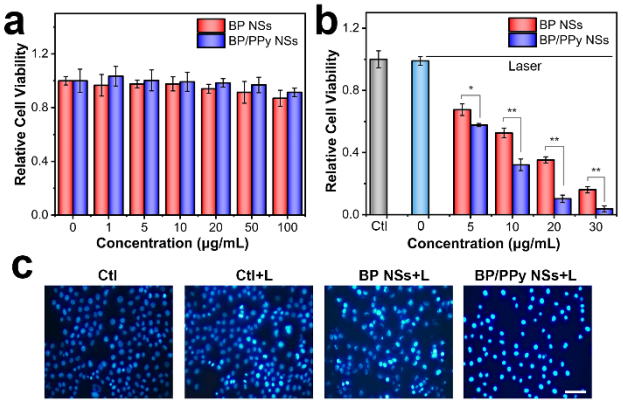

Fig. 4 a) The relative cell viability of 4T1 cells incubated with BP-based nanomaterials at different concentrations for 24 h. Data are presented as mean ± SD. b) *In vitro* NIR photothermal effect of BP-based nanomaterials on cancer cells. Data are presented as mean ± SD; *P<0.05, **P<0.01 vs. BP NSs group. c) Fluorescence photomicrographs of 4T1 cells after treatment, stained with Hoechst 33258. (Scale bar: 100 μm).

3.3 Cytotoxicity Assessments of Nanomaterials

Classic MTT assay was carried out to evaluate the cytotoxicity of BP-based nanomaterials. Fig. 4a demonstrates the cell viability of 4T1 breast cancer cells incubated with BP NSs or BP/PPy NSs at various concentrations ranging from 0 to 100 μg/mL for 24 h. No obvious decrease in cellular viability is noticed after the 4T1 cells are exposed to the nanomaterials. More than 90% of the cancer cells are alive when the concentration of nanostructures increases to 100 μg/mL, revealing the good biocompatibilities.

3.4 *In vitro* Photothermal Therapy

We further investigated the *in vitro* photothermal effect of BP/PPy NSs. As shown in Fig. 4b, the relative cell viability of 4T1 cells in the Control group or Laser group was almost 100%, which means that the inhibitory effect of laser irradiation alone on cell proliferation is not obvious. However, remarkable and concentration-dependent death is noticed in the 4T1 cells containing BP NSs or BP/PPy NSs after NIR laser irradiation. Compared to the cells incubated in the BP NSs, the 4T1 cells incubated with the same concentration of BP/PPy NSs suffer from more severely photothermal damage. It was shown that 97% of the cancer cells are destroyed after incubating with 30 μg/mL BP/PPy NSs, while more than 20% of 4T1 cells still alive in the BP NSs + Laser group. Although both BP NSs and BP/PPy NSs trigger intensive NIR photothermal ablation of cancer cells, less dosage of BP/PPy NSs is needed to acquire the same NIR PTT effect as that induced by BP NSs. The result indicates the better potential of BP/PPy NSs for NIR photothermal ablation of cancer cells.

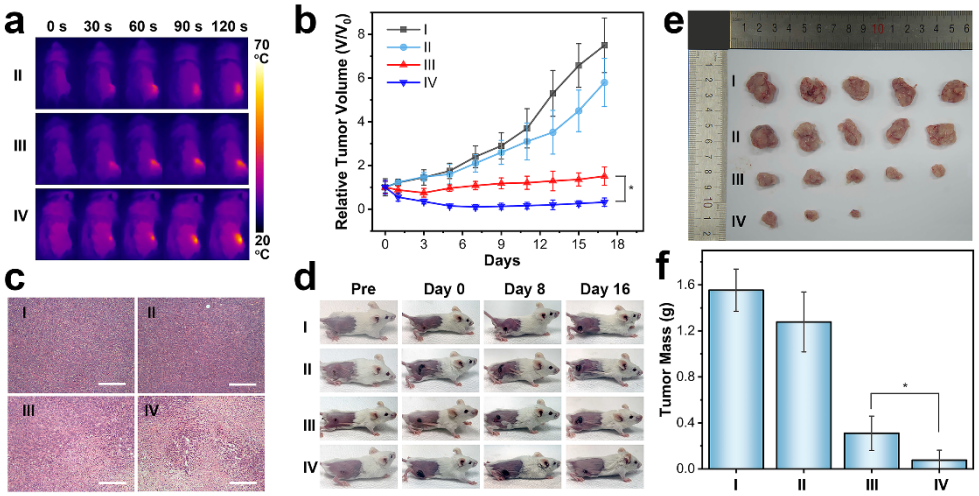

Fig. 5 a) Infrared thermal images of 4T1 tumor-bearing mice irradiated under 808 nm laser (2.0 W/cm^2) for 2 min. b) Tumor growth curves in different groups. Data are presented as mean ± SD; *P<0.05 vs. BP NSs group. c) Micrographs of H&E stained tumor tissues obtained from different groups (Scale bar: 100 μm). d) Representative photographs of tumor-bearing mice. e) Photographs of the tumors collected from different groups mice at the end of treatment. f) Average weights of the tumors collected from different groups. Data are presented as mean ± SD; *P<0.05 vs. BP NSs group. I, II, III and IV represent the Control group, PBS + Laser group, BP NSs + Laser group and BP/PPy NSs + Laser group, respectively.

In order to research on the apoptosis of the 4T1 cells, the cells were stained with Hoechst 33258 dye, a DNA-binding fluorochrome, after NIR treatment. From the Fig. 4c, it can be seen that the cells in the Control group emit light blue fluorescence and display uniform spherical nuclei. Similarly, there is no significant morphological change in the Laser group. However, a large number of irregular granules with bright blue luminescence are observed in the cells treated with BP NSs after laser exposure, which can be ascribed to the DNA fragmentation and chromatin condensation during apoptosis. This phenomenon is more serious in the BP/PPy NSs + Laser group, further confirming the improved NIR PTT capability of

the nanohybrids (Fig. S4†). The comparative photothermal experiments between PPy NPs and BP/PPy NSs were also carried out, which testifies the superior NIR PTT effect of on cancer cells BP/PPy NSs compared to their single components (Fig. S5†).

3.5 *In vivo* Photothermal Therapy

The *in vivo* antitumor effect of BP/PPy NSs was finally performed in tumor-bearing mice. The temperature changes of the tumors during laser irradiation were monitored by an infrared thermal imaging camera. The temperature of BP/PPy NSs injected tumor region increases by 50 °C after 2 min of NIR laser irradiation, which is completely sufficient to kill the tumor *in vivo*. In contrast, the tumor temperature of mice treated with BP NSs increases from 30 to 55 °C, which is significantly lower than that in BP/PPy NSs + Laser group. But the tumor temperature of mice in the PBS + Laser group only increases by 3 °C (Fig. 5a). The *in vivo* NIR photothermal effect was firstly measured by the histology analysis at 24 h after the laser treatment when the one of the tumors per group was extracted for hematoxylin and eosin (H&E) staining. As described in Fig. 5c, no significant morphological changes of the tumor cells are observed in control groups, whereas the cancer cells are severely damaged in the BP nanostructures treated mice.

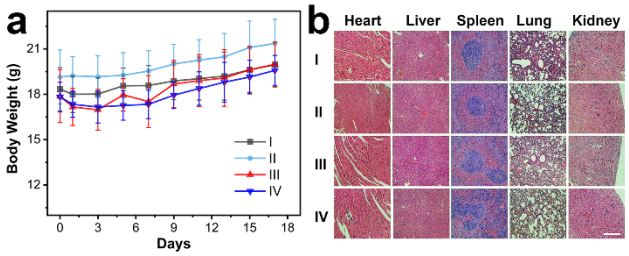

Fig. 6 a) Mean body weights of mice in various groups. b) Micrographs of H&E stained major organs obtained from different groups (Scale bar: 200 μm). I, II, III and IV represent the Control group, PBS + Laser group, BP NSs + Laser group and BP/PPy NSs + Laser group, respectively.

To further reveal the *in vivo* therapeutic efficiency after different treatments, the tumor sizes were evaluated by a digital caliper. As shown in the Fig. 5b, the tumor volumes of the mice in the Control group and PBS + Laser group grow rapid during the full observation process, indicating that laser treatment alone is inadequate to inhibit the tumor growth under our experimental parameters. While the tumor volumes of mice in the BP NSs + Laser group or BP/PPy NSs + Laser group are gradually decrease after NIR laser treatment. And the tumors in the two groups are effectively eliminated with only small black scars left at the tumor sites after 17 days' observation (Fig. 5d). The tumors undergone BP NSs and laser treatment display the obviously smaller sizes in comparison with that in control groups (Fig. 5b and e), showing the good antitumor effect of BP nanostructures. BP/PPy NSs combined with 808 nm laser exposure demonstrates the most effective tumor growth inhibition effect, as the tumors in this group are largely eliminated after treatment, only three small tumors are observed after dissection at the end of the experiment (Fig. 5e). The mean weight of tumor also verifies the enhanced *in vivo* antitumor effect of BP/PPy NSs based NIR PTT (Fig. 5f).

The toxic side effect usually leads to weight loss. As shown in Fig. 6a, there are no significant body weight losses in the all groups, indicating the low toxicities of the nanomaterials. To further assess the *in vivo* toxicity, mice were sacrificed 17 days after photothermal treatment, and the major organs of mice were sliced, and then stained by H&E for histology analysis. Fig. 6b illustrates the H&E stained images of major organs including heart, liver, spleen, lung and kidney, which exhibit no visible damage, suggesting the promise of BP/PPy NSs as biocompatible nanoagent for *in vivo* high-performance NIR photothermal therapy.

4. Conclusions

In summary, BP/PPy NSs have been prepared by facile strategy. The nanohybrids gather the double optical characteristics of the two components (BP NSs and PPy NPs), which exhibit an evidently improved light absorption in NIR region. The NIR photothermal transduction efficiency of BP/PPy NSs is calculated to be 62.2%, much higher than that of BP NSs (31.8%), indicating a less dosage of nanocomposites is needed for an effective PTT. *In vitro* and *in vivo* experiments have proven the enhanced NIR photothermal antitumor effect of BP/PPy NSs. The high-performance therapeutic application of this nanohybirds opens up a new perspective for BP-based nanomedicine.

Conflicts of interest

There are no conflicts to declare.

Acknowledgements

This work is supported by the National Natural Science Foundation of China (61675072, 11874021, 21505047, 61335011, 31300691 and 61275187), the Natural Science Foundation of Guangdong Province of China (2014A030311024), the Science and Technology Project of Guangdong Province of China (2017A020215059).

Notes and references

1 B. Thierry, *Curr. Drug Deliv.*, 2009, 6, 391.
2 D. J. Bharali and S. A. Mousa, *Pharmacol. Therapeut.*, 2010, 128, 324.
3 C. Minelli, S. B. Lowe and M. M. Stevens, *Small*, 2010, 6, 2336.
4 H. S. Jung, P. Verwilst, A. Sharma, J. Shin, J. L. Sessler and J. S. Kim, *Chem. Soc. Rev.*, 2018, 47, 2280.
5 D. de Melo-Diogo, C. Pais-Silva, D. R. Dias, A. F. Moreira and I. J. Correia, *Adv. Healthc. Mater.*, 2017, 6, 1700073.
6 W. Tao, X. Ji, X. Xu, M. A. Islam, Z. Li, S. Chen, P. E. Saw, H. Zhang, Z. Bharwani, Z. Guo, J. Shi and O. C. Farokhzad, *Angew. Chem. Int. Ed.*, 2017, 56, 11896.
7 A. K. Parchur, G. Sharma, J. M. Jagtap, V. R. Gogineni, P. S. LaViolette, M. J. Flister, S. B. White and A. Joshi, *ACS Nano*, 2018, 12, 6597.

8 J. Zhou, Y. Jiang, S. Hou, P. K. Upputuri, D. Wu, J. Li, P. Wang, X. Zhen, M. Pramanik, K. Pu and H. Duan, *ACS Nano*, 2018, 12, 2643.
9 K. Yang, S. A. Zhang, G. X. Zhang, X. M. Sun, S. T. Lee and Z. A. Liu, *Nano Lett.*, 2010, 10, 3318.
10 F. Yin, K. Hu, Y. Chen, M. Yu, D. Wang, Q. Wang, K. T. Yong, F. Lu, Y. Liang and Z. Li, *Theranostics*, 2017, 7, 1133.
11 Z. Liu, B. Ye, M. Jin, H. Chen, H. Zhong, X. Wang and Z. Guo, *Nanoscale*, 2015, 7, 6754.
12 X. Wang, Y. Ma, X. Sheng, Y. Wang and H. Xu, *Nano Lett.*, 2018, 18, 2217.
13 C. Yue, P. Liu, M. Zheng, P. Zhao, Y. Wang, Y. Ma and L. Cai, *Biomaterials*, 2013, 34, 6853.
14 J. Peng, L. Zhao, X. Zhu, Y. Sun, W. Feng, Y. Gao, L. Wang and F. Li, *Biomaterials*, 2013, 34, 7905.
15 L. Li, Y. Yu, G. J. Ye, Q. Ge, X. Ou, H. Wu, D. Feng, X. H. Chen and Y. Zhang, *Nat. Nanotechnol.*, 2014, 9, 372.
16 A. Hirsch and F. Hauke, *Angew. Chem. Int. Ed.*, 2018, 57, 4338.
17 R. Gui, H. Jin, Z. Wang and J. Li, *Chem. Soc. Rev.*, 2018, 47, 6795.
18 J. R. Choi, K. W. Yong, J. Y. Choi, A. Nilghaz, Y. Lin, J. Xu and X. Lu, *Theranostics*, 2018, 8, 1005.
19 H. Wang, X. Yang, W. Shao, S. Chen, J. Xie, X. Zhang, J. Wang and Y. Xie, *J. Am. Chem. Soc.*, 2015, 137, 11376.
20 J. Shao, H. Xie, H. Huang, Z. Li, Z. Sun, Y. Xu, Q. Xiao, X.-F. Yu, Y. Zhao, H. Zhang, H. Wang and P. K. Chu, *Nat. Commun.*, 2016, 7, 12967.
21 X. Qian, Z. Gu and Y. Chen, *Mater. Horiz.*, 2017, 4, 800.
22 Z. Sun, H. Xie, S. Tang, X. F. Yu, Z. Guo, J. Shao, H. Zhang, H. Huang, H. Wang and P. K. Chu, *Angew. Chem. Int. Ed.*, 2015, 54, 11526.
23 C. Xing, S. Chen, M. Qiu, X. Liang, Q. Liu, Q. Zou, Z. Li, Z. Xie, D. Wang, B. Dong, L. Liu, D. Fan and H. Zhang, *Adv. Healthc. Mater.*, 2018, 7, e1701510.
24 L. Deng, Y. Xu, C. Sun, B. Yun, Q. Sun, C. Zhao and Z. Li, *Sci. Bull.*, 2018, 63, 917.
25 B. Yang, J. Yin, Y. Chen, S. Pan, H. Yao, Y. Gao and J. Shi, *Adv. Mater.*, 2018, 30, 1705611.
26 W. Chen, J. Ouyang, H. Liu, M. Chen, K. Zeng, J. Sheng, Z. Liu, Y. Han, L. Wang, J. Li, L. Deng, Y. N. Liu and S. Guo, *Adv. Mater.*, 2017, 29, 1603864.
27 Y. Li, Z. Liu, Y. Hou, G. Yang, X. Fei, H. Zhao, Y. Guo, C. Su, Z. Wang, H. Zhong, Z. Zhuang and Z. Guo, *ACS Appl. Mater. Interfaces*, 2017, 9, 25098-25106.
28 W. Tao, X. Zhu, X. Yu, X. Zeng, Q. Xiao, X. Zhang, X. Ji, X. Wang, J. Shi, H. Zhang and L. Mei, *Adv. Mater.*, 2017, 29, 1603276.
29 M. Qiu, W. X. Ren, T. Jeong, M. Won, G. Y. Park, D. K. Sang, L. P. Liu, H. Zhang and J. S. Kim, *Chem. Soc. Rev.*, 2018, 47, 5588.
30 M. Qiu, D. Wang, W. Liang, L. Liu, Y. Zhang, X. Chen, D. K. Sang, C. Xing, Z. Li, B. Dong, F. Xing, D. Fan, S. Bao, H. Zhang and Y. Cao, *Proc. Natl. Acad. Sci. U. S. A.*, 2018, 115, 501.
31 G. Yang, Z. Liu, Y. Li, Y. Hou, X. Fei, C. Su, S. Wang, Z. Zhuang and Z. Guo, *Biomater. Sci.*, 2017, 5, 2048.
32 N. M. Latiff, W. Z. Teo, Z. Sofer, A. C. Fisher and M. Pumera, *Chemistry*, 2015, 21, 13991.
33 G. Qu, W. Liu, Y. Zhao, J. Gao, T. Xia, J. Shi, L. Hu, W. Zhou, J. Gao, H. Wang, Q. Luo, Q. Zhou, S. Liu, X. F. Yu and G. Jiang, *Angew. Chem. Int. Ed.*, 2017, 56, 14488.
34 J. Mo, Q. Xie, W. Wei and J. Zhao, *Nat. Commun.*, 2018, 9, 2480.
35 X. Zhang, Z. Zhang, S. Zhang, D. Li, W. Ma, C. Ma, F. Wu, Q. Zhao, Q. Yan and B. Xing, *Small*, 2017, 13, 1701210.
36 Q. Tian, Q. Wang, K. X. Yao, B. Teng, J. Zhang, S. Yang and Y. Han, *Small*, 2014, 10, 1063.
37 Z. Zha, X. Yue, Q. Ren and Z. Dai, *Adv. Mater.*, 2013, 25, 777.
38 K. Yang, H. Xu, L. Cheng, C. Sun, J. Wang and Z. Liu, *Adv. Mater.*, 2012, 24, 5586.
39 J.-Y. Hong, H. Yoon and J. Jang, *Small*, 2010, 6, 679.
40 M. Chen, X. Fang, S. Tang and N. Zheng, *Chem. Commun.*, 2012, 48, 8934.
41 A. Ramanaviciene, A. Kausaite, S. Tautkus and A. Ramanavicius, *J. Pharm. Pharmacol.*, 2007, 59, 311.
42 X. Wang, X. Gu, C. Yuan, S. Chen, P. Zhang, T. Zhang, J. Yao, F. Chen and G. Chen, *J. Biomed. Mater. Res. A*, 2004, 68A, 411.
43 Y. Furukawa, S. Tazawa, Y. Fujii and I. Harada, *Synth. Met.*, 1988, 24, 329.
44 L. Zhang, Y. Chen, Z. Li, L. Li, P. Saint-Cricq, C. Li, J. Lin, C. Wang, Z. Su and J. I. Zink, *Angew. Chem. Int. Ed.*, 2016, 55, 2118.
45 C. Sun, L. Wen, J. Zeng, Y. Wang, Q. Sun, L. Deng, C. Zhao and Z. Li, *Biomaterials*, 2016, 91, 81.